Hindawi Publishing Corporation
Journal of Nanomaterials
Volume 2011, Article ID 547103, 7 pages
doi:10.1155/2011/547103

Research Article

Preparation of Nanoporous TiO_2 Electrodes for Dye-Sensitized Solar Cells

Hsiue-Hsyan Wang,[1,2] Chaochin Su,[1] Huei-Siou Chen,[1] Yi-Cheng Liu,[1] Yi-Wen Hsu,[1] Nai-Mu Hsu,[3] and Wen-Ren Li[3]

[1] *Institute of Organic and Polymeric Materials, National Taipei University of Technology, Taipei 10608, Taiwan*
[2] *Department of Chemical and Materials Engineering, National Ilan University, 1, Sec.1, Shen-Lung Road, I-Lan 260, Taiwan*
[3] *Department of Chemistry, National Central University, Chung-Li 32001, Taiwan*

Correspondence should be addressed to Chaochin Su, f10913@ntut.edu.tw and Wen-Ren Li, ch01@ncu.edu.tw

Received 20 May 2010; Revised 19 August 2010; Accepted 24 August 2010

Academic Editor: William W. Yu

Nano-porous TiO_2 thin films have been widely used as the working electrodes in dye-sensitized solar cells (DSSCs). In this work, the phase-pure anatase TiO_2 (a-TiO_2) and rutile TiO_2 (r-TiO_2) have been prepared using hydrothermal processes. The investigation of photo-to-electron conversion efficiency of DSSCs fabricated from mixed-TiO_2 with a-TiO_2 and r-TiO_2 ratio of 80 : 20 (A8R2) was performed and compared to that from commercial TiO_2 (DP-25). The results showed higher efficiency of DSSC for A8R2 cells with same dependence of cell efficiency on the film thickness for both A8R2 and DP-25 cells. The best efficiency obtained in this work is 5.2% from A8R2 cell with TiO_2 film thickness of 12.0 μm. The correlation between the TiO_2 films thickness and photoelectron chemical properties of DSSCs fabricated from A8R2 and DP-25 was compared and discussed.

1. Introduction

Worldwide scientific community has invested much attention in dye sensitized solar cells (DSSCs) with possibilities of high energy conversion efficiency and low fabrication cost [1]. In DSSC, titanium dioxide (TiO_2) is one of the most promising materials used for nano-porous thin film due to its appropriate energy levels, dye adsorption ability, low cost, and easy preparation [2]. Extensive research on the photochemistry and photophysics of TiO_2-based DSSCs has shown that the light harvesting efficiency of TiO_2 is influenced by its crystalline phase, particle size, surface area, dye affinity, and film porosity. TiO_2 exists in two major phases: anatase and rutile. The anatase phase (a-TiO_2) gained much attention due to its more active surface chemistry and smaller particles for more dye adsorption. Anatase is metastable and can be transformed irreversibly to thermodynamically more stable and condense rutile phase at higher temperature. The rutile phase TiO_2 (r-TiO_2), due to the high refractive index, has excellent light-scattering characteristics, which is a profitable property of the perspective of effective light harvesting. Combination of anatase and rutile TiO_2 can be more effective than the pure phase owing to the electron-holes separation at the interface between phases and the formation of inter-band gap trap which may influence interparticle carrier transportation. The commercial Degussa P-25 TiO_2 (DP-25) composed of a-TiO_2 and r-TiO_2 at a ratio of 80 : 20 is known to be one of the most active photocatalysts due to the synergic effect [3]. In this paper, the phase pure a-TiO_2 and r-TiO_2 nanoparticles were first synthesized [4, 5]. The photoanodes from mixed-TiO_2 with a-TiO_2-to-r-TiO_2 ratio of 80 : 20 (A8R2) which resemble the phase ratio in DP-25 were then fabricated. Finally, the film characteristics and the DSSC performance of the A8R2 photoanodes were investigated and compared to those made of commercial DP-25.

2. Experimental Details

2.1. Preparation and Characterization of a-TiO_2, r-TiO_2, and Spin-Coated TiO_2 Electrodes. The preparation of TiO_2

nanoparticles involves controlled hydrolysis of Ti precursor followed by peptization. Detailed descriptions of the temperature dependent TiO_2 nanoparticles formation can be found in our previous works [6, 7]. Briefly, titanium (IV) n-butoxide (TNB) was mixed with 2 M acetic acid (for a-TiO_2) or 3 M hydrogen chloride (for r-TiO_2) at room temperature and carefully stirred until a translucent TiO_2 sol was obtained. The TiO_2 sol was then transferred to a Teflon-lined autoclave to perform the hydrothermal treatment at 200°C for 5 h (for a-TiO_2) or 220°C for 8 h (for r-TiO_2) followed by drying at 150°C for 8 h. These procedures resulted in the formation of oval-shaped a-TiO_2 and bar-shaped r-TiO_2 (see below). The TiO_2 samples were characterized by transmission electron microscopy (TEM, Hitachi) for particle shape and size, X-ray diffraction (XRD, Japan MAC Science) for crystal phase and domain size, and Brunauer, Emmett and Teller method (BET, Micromeritics Gemini V) for surface area analysis.

The TiO_2 films were made by spreading TiO_2 pastes on the fluorine-doped SnO_2 conducting glass (FTO, Solaronix, sheet resistance 8 Ω/□) by spin coating technique. Two kinds of TiO_2 pastes containing A8R2 and DP-25 were prepared by mixing-grounding the TiO_2 sample with distilled water, acetylacetone, and Triton X-100. Extensive stirring and sonication was proceeded to ensure complete dispersion of TiO_2 nanoparticles and to facilitate the spreading of the colloid on FTO. Droplets of each paste were placed onto the FTO substrate mounted on the turning table of a spin coater (IVY Semiconductor). Adhesive tapes were placed on the edges of FTO to form a guide for spreading the pastes with spin rate of 1000 rpm. After drying in air the TiO_2 electrodes were heated at 100°C for 15 min followed by annealing at 450°C for 30 min. The resulted electrodes were cooled to 80°C and immediately soaked in a 0.3 mM of solution of N719 dye in ethanol for overnight. Thickness of the TiO_2 film was controlled by multiple coating processes in which the coated substrates were subjected repeatedly to spin-coating and drying steps. The thickness of TiO_2 films were measured by an Alpha-step profiler (Perthometer S2). The surface morphology and crystal phase of TiO_2 films were characterized by SEM (Hitachi S-2400) and XRD (PANalytical X'Pert PRO MPD), respectively.

2.2. Dye-Sensitized Solar Cell Assembly and Performance Measurement. To assemble the DSSCs, the electrolyte of LiI (0.1 M), I_2 (0.05 M), 1,2-dimethyl-3-propyl imidazolium iodide (0.5 M), and 4-tert-butylpyridine (0.5 M) in acetonitrile was applied to the Pt counter electrodes (20 nm on FTO) which were placed over the N719-adsorbed TiO_2 electrodes. The edges of the cell were sealed with a 50 μm polyimide tape spacer. The active cell area studied in this work is 0.25 cm^2. The photocurrent-voltage characteristics were performed using a Keithley model 2400 source measuring unit. A solar simulator with 300 W Xenon lamp (Oriel) served as a light source, and its light intensity was adjusted by using an NREL-calibrated monocrystalline Silica solar cell for AM1.5 radiation. The electron transport properties were investigated using electrochemical impedance spectroscopy (EIS) with 10 mV alternative signal in the frequency range of 10^{-2}–10^5 Hz. The amount of adsorbed dye was determined by desorbing the dye from TiO_2 into a solution of 0.1 M NaOH and analyzed by UV-visible spectrophotometer (JASCO V-630).

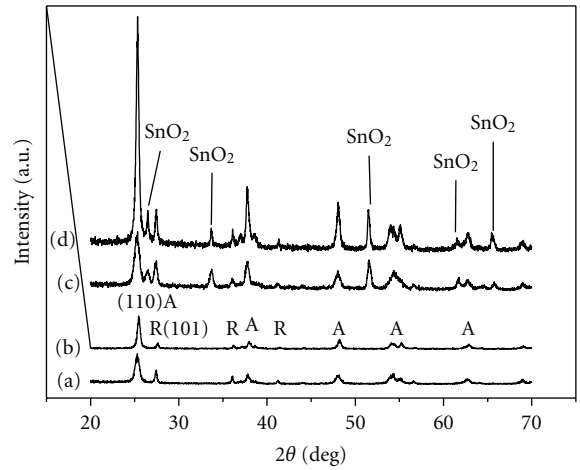

Figure 1: A series of XRD patterns for A8R2 powder (a), DP-25 powder (b), A8R2 film (c), and DP-25 film (d).

3. Results and Discussion

3.1. Preparation and Characterization of a-TiO_2, r-TiO_2, and Mixed-Phase TiO_2 Photoelectrode. The parameter-controlled sol-hydrothermal reactions employed in the present work led to the formation of a-TiO_2 and r-TiO_2 nanocrystallites. Various kinds of techniques were used for characterization of the products which was demonstrated in our previous works [6, 8]. After mixing a-TiO_2 with r-TiO_2 and spin-coating on FTO substrate, a porous TiO_2 film was obtained. Figure 1 shows the XRD patterns of the A8R2 powder (Figure 1(a)) and A8R2 film (Figure 1(c)). The diffraction patterns of DP-25 powder (Figure 1(b)) and DP-25 film (Figure 1(d)) are also shown for comparison. The XRD pattern of A8R2 film exhibited peaks corresponding to anatase and rutile phase indicating the presence of stable mixed-phase TiO_2 film after 30 min calcination at 450°C. Several peaks appear at $2(\theta) = 26.6$, 33.9, and 51.8 of Figures 1(c) and 1(d) which are due-to-SnO_2 from FTO substrate. The phase ratio of a-TiO_2 and r-TiO_2 is calculated from the equation of $F_r = 1.26I_r/(I_a + 1.26I_r)$, where I_r and I_a are the strongest intensities of rutile (110) and anatase (101) peaks, respectively. The calculated a-TiO_2 : r-TiO_2 ratio on A8R2 film is 63 : 37 which is deviated from the original ratio for mixed powder samples prior to calcination. The lower anatase content in calcined A8R2 film designates the possibility of phase transformation from anatase to rutile (A → R) upon calcination [9]. Similar transformation also occurs on the spin-coated DP-25 film in which the final anatase to rutile ratio is 73.4 : 26.5. Note that the A8R2 sample holds the higher extent of A → R compared to DP-25 due to the more compact arrangement of a-TiO_2 in A8R2 allowing the facile phase transformation (see below).

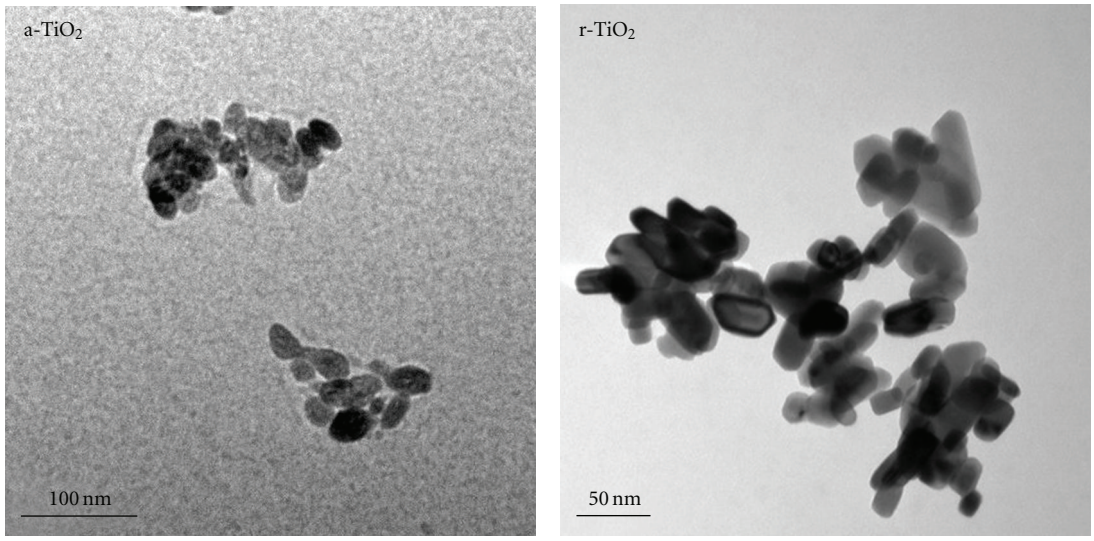

(a) (b)

Figure 2: TEM micrographs of TiO_2 samples: anatase TiO_2 (a-TiO_2 (a)) and rutile TiO_2 (r-TiO_2 (b)).

The phase ratio and crystallite sizes of a-TiO_2 and r-TiO_2 in A8R2 and DP-25 calculated by Scherrer equation are summarized in Table 1.

Figure 2 shows the TEM micrograph of pure a-TiO_2 (b) with distinct irregular oval structure and r-TiO_2 (a) with characteristic nanobar structure. The average of particle size is ~16 nm for a-TiO_2 and 40 × 20 nm in width × length for r-TiO_2. The DP-25 TiO_2 nanoparticles are polygonal in shape with average size of 30 nm (not shown). The particle size of nanocrystals can also be estimated from BET surface area measurement. The a-TiO_2, r-TiO_2, and DP-25 nanoparticles possess specific surface area of 116, 27, and 50 m^2/g, respectively. Based on an assumption of all anatase phase spherical particles and use of TiO_2 solid density of 3.84 g/cm^3 to convert the BET specific surface areas to particle diameters, the corresponding particle dimension for a-TiO_2, r-TiO_2, and DP-25 is 13, 56, and 29 nm, respectively, which is consistent with the TEM size measurement. The smaller particle size of a-TiO_2 in A8R2 is on account of the more dense and compact structure of A8R2 film compared to the DP-25 film (see below SEM images). The results of TiO_2 particle size derived from TEM and BET are also summarized in Table 1 and compared with the crystalline size obtained from XRD. The results show good agreement in TiO_2 particle size within the experimental error.

The spin-coated A8R2 films appeared to be smooth under visual inspection although the film showed some inhomogeneity at the edges. The SEM micrograph of TiO_2 film made of A8R2 sample (Figure 3(a)) shows a rough surface layer containing large TiO_2 chunks in which the individual TiO_2 particles are hardly visible. The chunk structure is likely formed through the aggregation of bar-shape r-TiO_2 arranged in a side-by-side configuration. Another possible reason for the appearance of irregular chunks on the A8R2 layer is the stress-induced surface rumpling caused by the fast cooling after 450°C calcination. The chunk-free and almost smooth area exhibits more compact structure than the DP-25 based film as shown in Figure 3(b). Presumably, this is due to the small a-TiO_2 particles forming the high density A8R2 film. It is also noted from Figure 3(b) that the film made from DP-25, even with high porosity, showed appearance of breaks which may influence the electron transport and result in lower cell efficiency than that of A8R2 (see below). The A8R2 nanoparticles, on the other hand, can restrict the constriction resulting in the continuous less-crack and porous films upon calcination. Nevertheless, for both TiO_2 films, the crack produced voids in the preceding layer can be filled by the A8R2 and DP-25 paste during the next spin-coating process.

3.2. Application of Mixed-Phase TiO_2 Photoelectrodes to DSSCs and the Photoelectrochemical Performance Measurement. The above prepared A8R2 and DP-25 photoelectrodes were used to fabricate the solar cells for photoelectrochemical performance study [10, 11]. Figure 4 showed the typical current-voltage characteristics of N719-sensitized DSSCs for various film thickness of A8R2 films (a) and DP-25 films (b). Table 2 lists the photoelectric data of the DSSCs in Figure 4 including the amount of dye adsorbed on TiO_2 (A_{dye}), the short-circuit photocurrent density (J_{sc}), the open circuit voltage (V_{OC}), the fill factor (FF), and the conversion efficiency (η). It is apparent that the DSSC performance largely depends on the TiO_2 film thickness because changing the film thickness changes A_{dye}, J_{sc}, and, η owing to the change of total TiO_2 surface area. To clarify relationship between the thickness, surface properties of the TiO_2 films, and the photoelectrochemical characteristics of the cells, comparison of η of DSSCs and the corresponded J_{sc} using A8R2 TiO_2 and DP-25 as a function of film thickness is plotted and shown in Figure 5(a). It is found that there is a parallel increase of efficiency for A8R2 cells (solid squares) and DP-25 cells (open squares) for TiO_2 film thickness

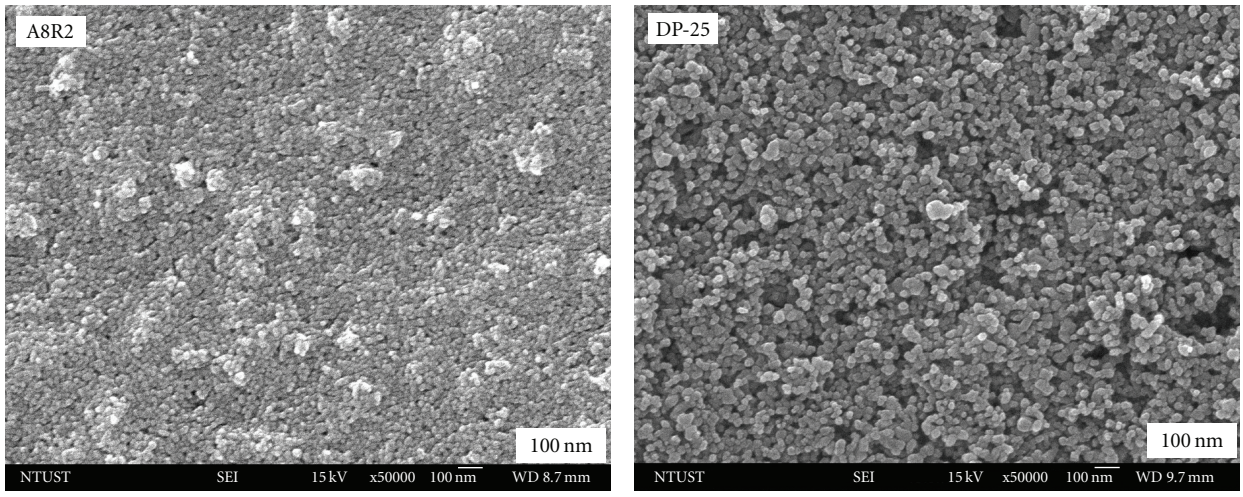

(a) (b)

Figure 3: Top-view SEM micrographs of A8R2 (a) and DP-25 (b) spin coated on FTO substrates.

Table 1: Phase ratio from XRD of TiO_2 samples (A8R2 and DP-25) before (powder) and after (film) calcination, comparison of TiO_2 crystallite size (A8R2 and DP-25) of anatase (A) and rutile (R) from XRD, and particle size (A8R2 and DP-25, powder only) obtained from TEM and BET.

TiO_2 Sample	Phase ratio (%)		Crystallite size (nm)		TEM (nm)	BET (nm)
A8R2 powder	80.4 (A[a])	20.0 (R[b])	14.8 (A)	26.0 (R)	16.0 (A)	13.0 (A)
A8R2 film	63.0 (A)	37.0 (R)	13.1 (A)	26.3 (R)	30×60 (R)	56 (R)
DP-25 powder	80.7 (A)	19.3 (R)	22.5 (A)	25.6 (R)	30	29
DP-25 film	73.4 (A)	26.5 (R)	22.6 (A)	27.3 (R)		

[a]A: anatase phase. [b]R: rutile phase.

up to $\sim 9\,\mu$m. Further increase in the thickness stabilizes the efficiency at an almost constant value upon increasing the thickness of TiO_2 thin films. The maximum efficiency acquired in DSSC using the A8R2 TiO_2 with film thickness of $12\,\mu$m was 5.20% with J_{sc} of 10.67 mA/cm^2, V_{OC} of 0.73 V, and FF of 0.69; while η of the cell using DP-25 with film thickness of $16\,\mu$m reached 3.76% with J_{sc} of 8.63 mA/cm^2, V_{OC} of 0.74 V, and FF of 0.59. The FF of DSSC is manipulated by device assembling technique which would affect the efficiency. Table 2 shows reasonable FF values compared with the other cases reported in the literatures [12, 13] and guarantee us a basic device fabrication technology.

It is generally believed that thicker TiO_2 film would uptake more N719 molecules leading to the enhancement in the photocurrent of the DSSC. As shown also in Figure 5(a), the influence of film thickness on J_{sc} of DSSCs constructed with A8R2 (solid triangles) and DP-25 (open triangles) demonstrates the consistent dependence of the film thickness on η. However, the variation of A_{dye} shows a continuous increase upon increasing of film thickness as shown in Figure 5(b) for both A8R2 (solid triangles) and DP-25 (solid squares). This result indicates the limited electron transport for thick films due to the increase of recombination centers and requisite path length of the injected electron to be collected by FTO. Moreover, when the TiO_2 films are thicker, the films become less transparent which is detrimental to the light harvesting as well as DSSC performance.

Based on Figure 5, the A8R2 cells in general have superior performance than DP-25 cells. The efficiency and current density from average of seven A8R2 cells present in Table 2 are $\sim$27.7% (η) and 29% (J_{sc}) higher than those from average of six DP-25 cells. Higher efficiency and current density might be attributed to, first, the higher amount of adsorbed N719 for the A8R2 cell, owing to larger surface area of A8R2 powder (71 and 50 m^2/g for A8R2 and DP-25, resp.) and more compact structure of A8R2 film (Figure 3). Higher UV absorption intensity of the N719 adsorbed on A8R2 film than DP-25 film (not shown) also supports this conclusion. Secondly, it could be due to the less cracks of A8R2 films (see above) which improved the short-circuit photocurrent [14]. Finally, with similar phase ratio of anatase to rutile TiO_2, the electron transport of A8R2 film containing the one dimension (1D) bar-shape r-TiO_2 is expected to be faster than the DP-25 film containing polygonal TiO_2. The electron transport properties of the DSSCs with TiO_2 electrodes made of A8R2 and DP-25 films were investigated by electrochemical impedance spectroscopy (EIS). According to the EIS spectra shown in Figure 6, the charge-transfer resistance at DP-25 electrode interface is larger than that at A8R2 interface. After the impedance data analysis by Zahner

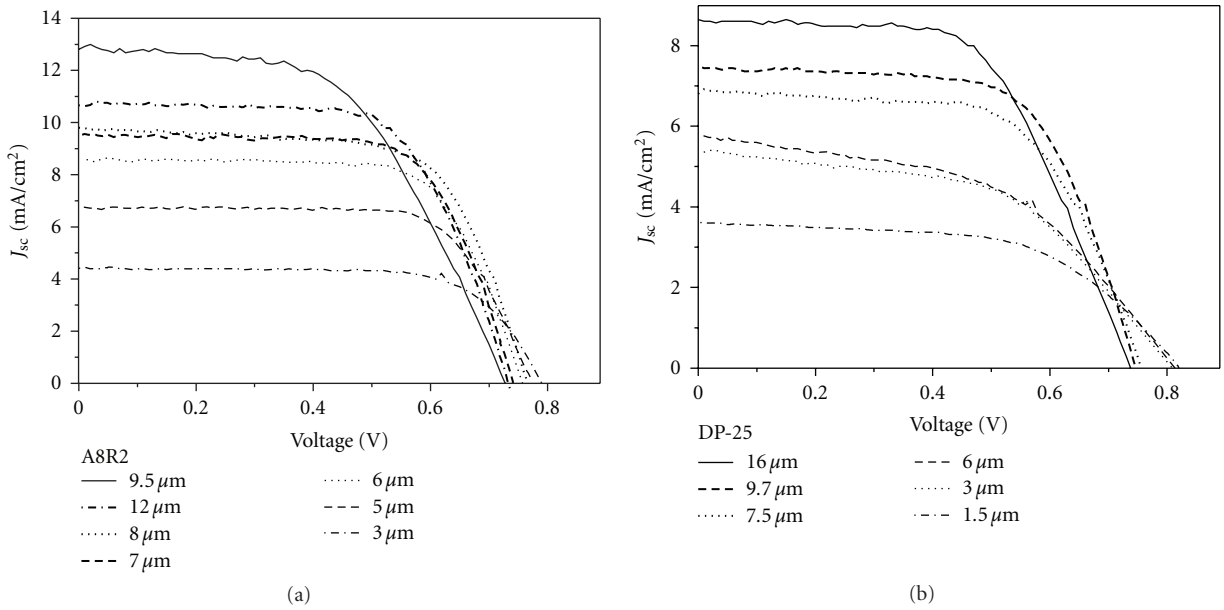

Figure 4: Photocurrent-voltage characteristics of DSSCs with different thicknesses of A8R2 films (a) and DP-25 films (b).

Table 2: I-V characteristic data for all DSSCs fabricated by A8R2 and DP-25 electrodes with various film thickness.

TiO_2 Sample	Thickness (μm)	A_{dye}[a] (μmole/cm^2)	J_{sc}[b] (mA/cm^2)	V_{OC}[c] (V)	FF[d]	η[e] (%)
A8R2-1	3.0	0.014	4.41	0.79	0.75	2.61
A8R2-2	5.0	0.043	6.71	0.77	0.72	3.71
A8R2-3	6.0	0.101	8.57	0.76	0.70	4.54
A8R2-4	7.0	0.110	9.53	0.74	0.69	4.89
A8R2-5	8.0	0.118	9.80	0.77	0.66	4.97
A8R2-6	9.5	0.159	10.50	0.74	0.67	4.92
A8R2-7	12.0	0.201	10.67	0.73	0.69	5.20
P25-1	1.5	0.022	3.43	0.82	0.56	1.69
P25-2	3.0	0.036	5.40	0.80	0.57	2.34
P25-3	6.0	0.059	5.93	0.80	0.54	2.38
P25-4	7.5	0.060	6.78	0.76	0.63	3.25
P25-5	9.7	0.064	7.49	0.75	0.64	3.61
P25-6	16.0	0.107	8.63	0.74	0.59	3.76

[a]A_{dye}: amount of dye adsorbed on TiO_2. [b]J_{sc}: short-circuit photocurrent density. [c]V_{OC}: open circuit voltage. [d]FF: fill factor. [e]η: cell efficiency.

software through fitting the data with appropriate equivalent circuit [15], the estimate electron transport resistance for DSSCs with DP-25 and A8R2 is 0.239 Ω and 0.105 Ω, respectively. This result is consistent with the superior efficiency of A8R2 cell than the DP-25 cell.

To confirm that the A8R2 cell has the optimized a-TiO_2-to-r-TiO_2 ratio for cell performance, we have fabricated DSSCs based on the mixed a-TiO_2 and r-TiO_2 composite films with weight ratio (wt%) of 9 : 1 (A9R1), 8 : 2 (A8R2) and 7 : 3 (A7R3). It was found that for the similar thickness of TiO_2 films, the A8R2 cell showed higher efficiency (η) by about 6.0% and 3.4% respectively, compared to A9R1 and A7R3 cells. With the increase of the r-TiO_2 content from A9R1 to A8R2, η was enhanced due to the faster electron transport rate as envisaged above. Upon further increase of r-TiO_2 content to A7R3, the cell efficiency decreased, presumably because less dye molecules had been adsorbed. This result could be attributed to the decrease of total surface area for sensitizers due to the smaller specific surface area of r-TiO_2 (27 m^2/g) compared to that of a-TiO_2 (116 m^2/g). A more precise fine-tuning of the a-TiO_2-to-r-TiO_2 ratio to optimize DSSC performance would require further experimental investigation.

4. Conclusion

Irregular oval-shape a-TiO_2 and bar-shape r-TiO_2 nanoparticles were prepared by hydrolysis and peptization of TNB followed by hydrothermal treatment. The cell efficiency of DSSCs made from mixed-phase A8R2 and DP-25 showed

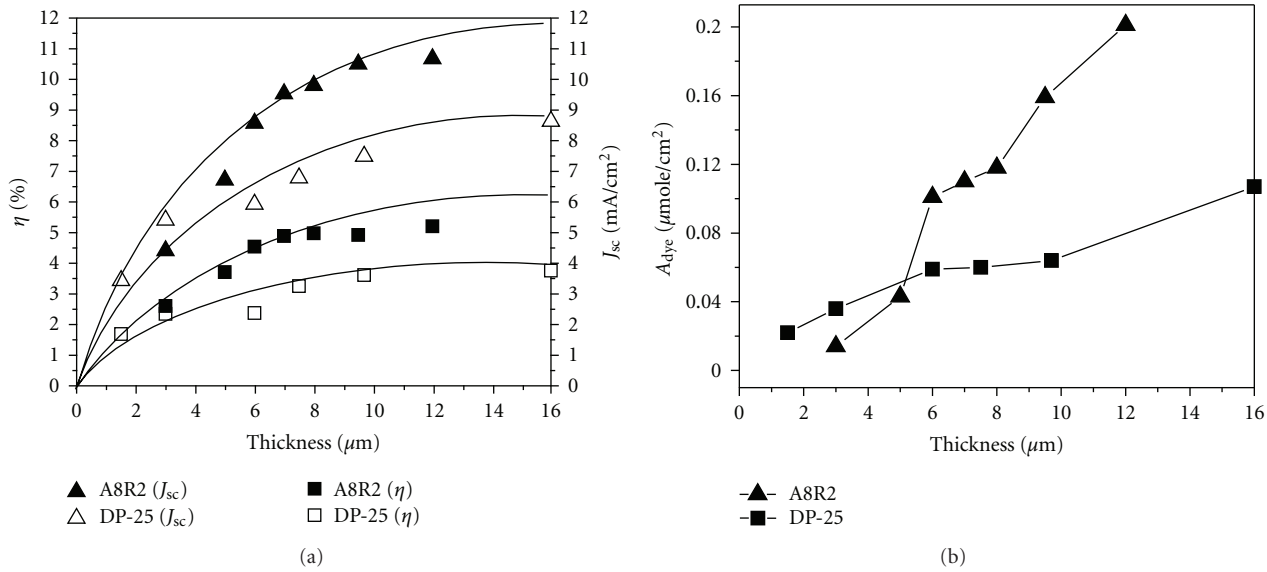

Figure 5: Influence of film thickness on conversion efficiency (η (a)), current density (J_{sc} (a)), and amount of adsorbed dye (A_{dye} (b)) on TiO_2 films.

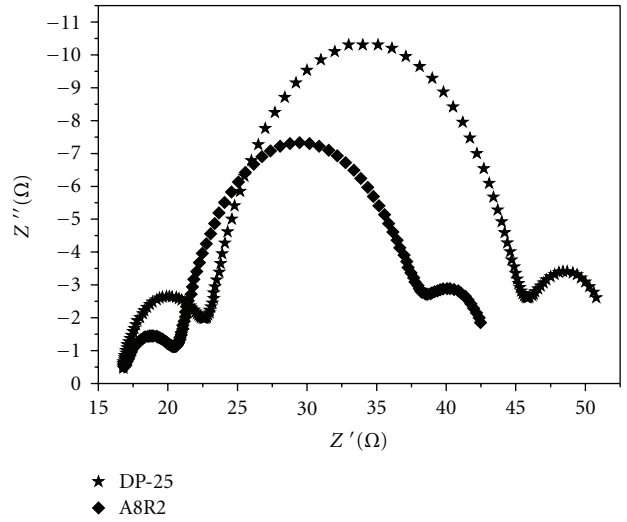

Figure 6: EIS spectra of the DSSCs made of DP-25 and A8R2 films.

the similar thickness dependence. The efficiency increases with film thickness and reaches a maximum plateau at thickness above ~9 μm. The A8R2 film shows more compact structure with consistent and superior DSSC performance than DP-25 cells. This could be due to the higher amount of adsorbed N719 on A8R2 film, less cracks of A8R2 film, and faster electron transport of A8R2 film containing the 1D bar-shape r-TiO_2.

Acknowledgment

The authors gratefully acknowledge the financial support of the National Science Council of Taiwan, Taiwan (Contract no. NSC96-2113-M-027-005-MY2 and NSC 96-2113-M-008-002-MY3).

References

[1] B. O'Regan and M. Grätzel, "A low-cost, high-efficiency solar cell based on dye-sensitized colloidal TiO_2 films," *Nature*, vol. 353, no. 6346, pp. 737–740, 1991.

[2] U. Diebold, "The surface science of titanium dioxide," *Surface Science Reports*, vol. 48, no. 5-8, pp. 53–229, 2003.

[3] N.-G. Park, J. Van de Lagemaat, and A. J. Frank, "Comparison of dye-sensitized rutile- and anatase-based TiO_2 solar cells," *Journal of Physical Chemistry B*, vol. 104, no. 38, pp. 8989–8994, 2000.

[4] C.-C. Wang and J. Y. Ying, "Sol-gel synthesis and hydrothermal processing of anatase and rutile titania nanocrystals," *Chemistry of Materials*, vol. 11, no. 11, pp. 3113–3120, 1999.

[5] H. Cheng, J. Ma, Z. Zhao, and L. Qi, "Hydrothermal preparation of uniform nanosize rutile and anatase particles," *Chemistry of Materials*, vol. 7, no. 4, pp. 663–671, 1995.

[6] H.-S. Chen, C. Su, J.-L. Chen, T.-Y. Yang, N.-M. Hsu, and W.-R. Li, "Preparation and characterization of pure rutile TiO_2 nanoparticles for photocatalytic study and thin films for dye-sensitized solar cells," *Journal of Nanomaterials*. In press.

[7] C. Su, C.-M. Tseng, L.-F. Chen, B.-H. You, B.-C. Hsu, and S.-S. Chen, "Sol-hydrothermal preparation and photocatalysis of titanium dioxide," *Thin Solid Films*, vol. 498, no. 1-2, pp. 259–265, 2006.

[8] H.-S. Chen, C. Su, C.-K. Lin, Y.-F. Hsieh, C.-K. Yang, and W.-R. Li, "Hydrothermal preparation of anatase TiO_2 nanoparticles for dye-sensitized solar cells," *Journal of Chemical Engineering of Japan*, vol. 42, supplement 1, pp. 36–42, 2009.

[9] Y. Hu, H.-L. Tsai, and C.-L. Huang, "Phase transformation of precipitated TiO_2 nanoparticles," *Materials Science and Engineering A*, vol. 344, no. 1-2, pp. 209–214, 2003.

[10] A. Fujishima and K. Honda, "Electrochemical photolysis of water at a semiconductor electrode," *Nature*, vol. 238, no. 5358, pp. 37–38, 1972.

[11] M. Grätzel, "Photoelectrochemical cells," *Nature*, vol. 414, no. 6861, pp. 338–344, 2001.

[12] Y. Guo, N.-H. Lee, H.-J. Oh et al., "Preparation of titanate nanotube thin film using hydrothermal method," *Thin Solid Films*, vol. 516, no. 23, pp. 8363–8371, 2008.

[13] M. C. Kao, H. Z. Chen, S. L. Young, C. Y. Kung, and C. C. Lin, "The effects of the thickness of TiO_2 films on the performance of dye-sensitized solar cells," *Thin Solid Films*, vol. 517, no. 17, pp. 5096–5099, 2009.

[14] L. Han, N. Koide, Y. Chiba, and T. Mitate, "Modeling of an equivalent circuit for dye-sensitized solar cells," *Applied Physics Letters*, vol. 84, no. 13, pp. 2433–2435, 2004.

[15] J.-J. Wu, G.-R. Chen, H.-H. Yang, C.-H. Ku, and J.-Y. Lai, "Effects of dye adsorption on the electron transport properties in ZnO-nanowire dye-sensitized solar cells," *Applied Physics Letters*, vol. 90, no. 21, Article ID 213109, 2007.